ARMY RESEARCH LABORATORY

The Influence of Propellant Deterrent Concentration Profile on Interior Ballistics Predictions Using Lumped-Parameter and Multiphase Flow Codes

by Albert W. Horst and Michael J. Nusca

ARL-TR-4713 **February 2009**

NOTICES

Disclaimers

The findings in this report are not to be construed as an official Department of the Army position unless so designated by other authorized documents.

Citation of manufacturer's or trade names does not constitute an official endorsement or approval of the use thereof.

Destroy this report when it is no longer needed. Do not return it to the originator.

Army Research Laboratory
Aberdeen Proving Ground, MD 21005-5066

ARL-TR-4713 **February 2009**

The Influence of Propellant Deterrent Concentration Profile on Interior Ballistics Predictions Using Lumped-Parameter and Multiphase Flow Codes

Albert W. Horst
American Systems

Michael J. Nusca
Weapons and Materials Research Directorate, ARL

REPORT DOCUMENTATION PAGE	Form Approved OMB No. 0704-0188

1. REPORT DATE *(DD-MM-YYYY)*	2. REPORT TYPE	3. DATES COVERED (From - To)
February 2009	Final	January 2007–April 2008

4. TITLE AND SUBTITLE
The Influence of Propellant Deterrent Concentration Profile on Interior Ballistics Predictions Using Lumped-Parameter and Multiphase Flow Codes

5a. CONTRACT NUMBER

5b. GRANT NUMBER

5c. PROGRAM ELEMENT NUMBER

6. AUTHOR(S)
Albert W. Horst* and Michael J. Nusca

5d. PROJECT NUMBER
622618H8000

5e. TASK NUMBER

5f. WORK UNIT NUMBER

7. PERFORMING ORGANIZATION NAME(S) AND ADDRESS(ES)
U.S. Army Research Laboratory
ATTN: AMSRD-ARL-WM-BD
Aberdeen Proving Ground, MD 21005-5066

8. PERFORMING ORGANIZATION REPORT NUMBER
ARL-TR-4713

9. SPONSORING/MONITORING AGENCY NAME(S) AND ADDRESS(ES)

10. SPONSOR/MONITOR'S ACRONYM(S)

11. SPONSOR/MONITOR'S REPORT NUMBER(S)

12. DISTRIBUTION/AVAILABILITY STATEMENT
Approved for public release; distribution is unlimited.

13. SUPPLEMENTARY NOTES
*American Systems, Aberdeen Proving Ground, MD 21001

14. ABSTRACT
Predictions of interior ballistics behavior of guns using simulation codes are highly dependent on the accuracy of the required inputs describing the gun, projectile, and often most difficult, the propellant and related charge characteristics (e.g., primer, case, and parasitic components). This problem is only exacerbated with more sophisticated codes requiring data on propellant ignitability and thermal and mechanical properties as well as the standard thermochemical and burning rate data. But even these last two requirements, common to all levels of interior ballistics codes, can be very difficult to meet for propellants with varying compositions, known commonly as deterred propellants. Long used for small arms propellants, deterred propellant concepts for larger-caliber guns are now under development as well. In this report, we examine the influence of two simple but extreme descriptions of deterrent concentration as a function of depth in a variety of granulations and using several levels of interior ballistics codes.

15. SUBJECT TERMS
CFD, multiphase flow, solid propellant, guns, deterred propellant

16. SECURITY CLASSIFICATION OF:			17. LIMITATION OF ABSTRACT	18. NUMBER OF PAGES	19a. NAME OF RESPONSIBLE PERSON
a. REPORT	b. ABSTRACT	c. THIS PAGE			Albert W. Horst
UNCLASSIFIED	UNCLASSIFIED	UNCLASSIFIED	UL	40	19b. TELEPHONE NUMBER (*Include area code*) 410-278-6108

Standard Form 298 (Rev. 8/98)
Prescribed by ANSI Std. Z39.18

Contents

List of Figures

INTENTIONALLY LEFT BLANK.

1. Background

The fundamental problem of the gun propelling charge designer can be simply stated as that of maximizing the transfer of chemical energy in a given propellant charge to kinetic energy of a projectile at muzzle exit. More specifically, one wants to raise the pressure acting on the base of the projectile as quickly as practical to some maximum level (defined by the various system constraints) and then maintain that pressure as close to that maximum level as possible until burnout as the projectile moves down the bore. The challenge can be quickly seen to be one of a competition between the production of gases from the burning propellant and the volume to put them in as the projectile moves down the bore. Typically, the pressure rises rapidly in the gun chamber until projectile motion generates new volume faster than the burning propellant does gases. In an attempt to increase the rate of gas production as the propellant burns, "progressive geometries" are typically used for large-caliber guns such that the burning surface increases as a function of burn distance (e.g., multiperforated grains).

Unfortunately, small arms generally require correspondingly small propellant grains so that they will be consumed in the much smaller timeframe available for the projectile to travel to exit. These small grain dimensions substantially increase the difficulty of, or even preclude, the possibility of manufacturing a high-quality, multiperforated configuration. Hence, an alternate means of achieving progressive mass generation profiles was devised: rather than increasing the burning surface with burn distance, simply increase the burning rate (and energy) of the propellant grain as a function of burn distance. By coating or impregnating the surface of the propellant grain with a lower energy material that penetrates the propellant for some distance, the desired depth-dependent burning rate and energy properties can be obtained. Numerous references exist on the effectiveness of various deterring materials and processes (*1*). Perhaps, the most well known are small arms ball propellants, which typically employ a simple spherical grain steeped in a deterrent material to provide the desired chemical gradient in the grain and rolled to an oblate spherical shape for better packing densities.

Historically, one problem has been to determine how to represent this gradient and its associated properties in gun interior ballistics codes so that performance could be predicted and grain parameters optimized. Therefore, the technique of blending propellant lots from batches with differing deterrent level and depth characteristics was developed to compensate for this difficulty. Measurement techniques have vastly improved but are still extremely labor-intensive, and blending continues to be a common production technique.

Today, however, propellant producers and charge designers are looking at many new approaches to achieving mass generation rate progressivity (*2*). Indeed, the St. Marks Powder Company is now exploiting a hybrid propellant concept for large-caliber guns involving the use of deterrents

and progressive grain geometries (*3*). Blending is still possible at these scales, but the ability to predict the influence of a specific deterrent profile on gun performance is clearly of interest to the charge design community.

2. Scope of Study

Granulations studied included deterred spherical ball propellant, deterred oblate spheres, deterred seven-perforated cylindrical grains, and seven-perforated cylindrical grains, with deterrent only on the outer cylindrical surface and ends (i.e., no deterrent on the walls of the perforations). Appropriate but generic gun configurations were selected for evaluation of each of these granulations: spherical balls in a 5.56-mm gun, oblate spheres in a 30-mm gun, and both seven-perforated configurations in a 120-mm gun.

Two representations were assumed for the deterrent concentration profile. First, a ramp profile was defined where the deterrent concentration is assumed to decrease linearly from a given surface level to a depth at which the assumed content was depleted. Second, a block profile was determined describing the same total deterrent content, but at a constant concentration level until depletion. The general procedure involved the development of algorithms that related surface concentration to penetration depth for a given total level of deterrent in the overall propellant formulation for each of the granulations considered. BLAKE code (*4*) calculations were then performed to determine thermochemical values for surface and core compositions. Burning rate coefficients were then assigned (exponents being held constant), using an assumption that the burning rate surface-to-core ratio was simply the square of the ratio of the corresponding impetus levels. Then, to provide a fair assessment of the impact of the two profiles on performance, surface deterrent levels for the block profiles were varied until a match in maximum pressure to those of the ramp profiles was achieved. Details are presented with each of the sets of calculations. Finally, to the degree possible, these sets of conditions were assessed using three levels of codes: the IBHVG2 lumped-parameter code; the one-dimensional (1-D) with area change, two-phase flow XKTC code; and the multidimensional, two-phase flow ARL NGEN3 code.

Briefly, IBHVG2 (*5*) provides a simple but useful lumped-parameter representation of the interior ballistics cycle. It embodies such assumptions as uniform and simultaneous ignition of the entire propellant charge, with combustion assumed to take place in a smoothly varying, well-stirred mixture, and the burning rate being determined by the instantaneous, space-mean chamber pressure. An assumed longitudinal pressure gradient is superimposed on the solution at each instant in time to appropriately reduce the pressure on the base of the projectile. While an

excellent tool for estimating overall performance of a gun, the study of ignition-induced pressure waves is clearly outside the physical scope of this model. However, all granulations described previously can be treated.

Next, the XKTC code (*6*) provides a quasi-1-D, macroscopic (with respect to individual grains), two-phase description of flow in the gun chamber, with the conservation laws formulated to neglect the effects of viscosity and heat conduction in the gas phase. Most importantly, gas and solid phases are coupled through heat transfer, combustion, and interphase drag; these processes are modeled using empirical correlations that relate the microphenomena to the average flow properties described by the governing equations. The igniter is either modeled explicitly or treated as a predetermined mass injection profile. Flame spreading follows primarily according to convection until the ignition temperature is reached, and combustion follows at a rate determined by the local pressure. Formulated as 1-D with area change representation, XKTC provides a first-level capability for treating the dynamics of the axial pressure field and its potential for causing potentially damaging overpressures. Unfortunately, no capability currently exists for treating deterrents except on all surfaces, precluding consideration of the final grain-type just described.

Finally, the NGEN code (*7–10*) is a multidimensional, multiphase computational fluid dynamics code that incorporates three-dimensional (3-D) continuum equations along with auxiliary relations into a modular code structure. On a sufficiently small scale of resolution in space and time, the components of the interior ballistics flow are represented by two-dimensional axisymmetric or fully 3-D balance equations for a multicomponent reacting mixture describing the conservation of mass, momentum, and energy. A macroscopic representation of the flow is adopted using these equations derived by a formal averaging technique applied to the microscopic flow. These equations require a number of constitutive laws for closure, including state equations, intergranular stresses, and interphase transfer (similar to those employed in the XKTC code). The numerical representation of these equations, as well as the numerical solution thereof, is based on a finite-volume discretization and high-order accurate, conservative numerical solution schemes. The spatial values of the dependent variables at each time step are determined by a numerical integration method, denoted the continuum flow solver (CFS), treating the continuous phase and certain of the discrete phases in an Eulerian fashion. The flux-corrected transport scheme (*11*) is a suitable basis for the CFS since the method is explicit and has been shown to adapt easily to massively parallel computer systems. The discrete phases are treated by a Lagrangian formulation, denoted the large particle integrator (LPI), tracking the particles (described next) explicitly and smoothes discontinuities associated with boundaries between propellants, yielding a nearly continuous distribution of porosity over the entire domain. The manner of coupling between the CFS and the LPI is through the attribution of properties (e.g., porosity and mass generation). The size of the grid, as well as the number of Lagrangian particles, is user prescribed. The solid propellant is modeled using Lagrange particles that regress, produce combustion product gases, and respond to gasdynamic and physical forces.

Individual grains, sticks, slab, and wrap layers are not resolved; rather each propellant medium is distributed within a specified region in the gun chamber. The constitutive laws that describe interphase drag, form-function, etc., assigned to these various media, determine preferred gas flow paths through the media (e.g., radial for disks and axial for sticks) and responses of the media to gasdynamic forces. Media regions that are encased in impermeable boundaries, which only yield to gasdynamic flow after a prescribed pressure differential and/or surface temperature is reached, act as rigid bodies within the chamber. The use of computational particles to represent the propellant charge permits a host of other modeling features that enhance the representation of charge details. The final grain type in our study—seven-perforated cylindrical grains with deterrent only on the outer cylindrical surface and ends (i.e., no deterrent on the walls of the perforations)—is outside the current scope of this code.

3. Computational Results – IBHVG2 Code/Spherical Ball Propellant

The first series of computations using the IBHVG2 interior ballistics code employed a deterred spherical ball propellant in a generic 5.56-mm gun as a subject. While input data are generally in accord with those describing an M855 cartridge, similar to those of a recent interior ballistics study (*12*), the current study required some revision of the treatment of the deterrent concentration profile. The overall concentration of deterrent in this and all subsequent calculations in this study was taken to be 5% of the total composition. The problem is then one of relating the depth of deterrent penetration to surface concentration for the ramp and block profiles described in the previous section.

Using the nomenclature given at the end of this report in the List of Symbols, Abbreviations, and Acronyms, the grain surface as a function of burn distance was as follows:

$$S(x) = 4\pi(r - x)^2 . \tag{1}$$

For the block deterrent concentration profile (i.e., constant value as a function of depth until depletion), the depth of penetration, surface concentration, and total mass of deterrent were related according to the following:

$$\int_0^{d_p} S(x)\rho C_s dx = m_d . \tag{2}$$

For the ramp deterrent concentration profile (i.e., linearly decreasing value from surface concentration to zero at depletion), the corresponding relationship was as follows:

$$\int_0^{d_p} S(x)\rho C_s (1 - x/d_p) dx = m_d . \tag{3}$$

It was also known that

$$m_d = \rho(C_t)(4/3)\pi r^3 . \tag{4}$$

Substituting equations 1 and 4 into equations 2 and 3 and performing the integrations, we obtained the following equations relating penetration depth, surface concentration, and total concentration of the deterrent for the block profile:

$$(d_p{}^3 / r^3) - (d_p{}^2 / r^2) + (d_p / r) = C_t / 3C_s , \tag{5}$$

and for the ramp profile,

$$(d_p{}^3 / 12r^3) - (d_p{}^2 / 3r^2) + (d_p / 2r) = C_t / 3C_s . \tag{6}$$

Equations 5 and 6 were then used to generate deterrent concentration profiles assuming a total concentration of 5% and a ramp distribution with a penetration depth of 0.065 mm and corresponding surface concentration of 14.05%; a block distribution with the same penetration depth of 0.065 mm and a corresponding surface concentration of 7.26%; and a block distribution of half the penetration depth, now 0.0325 mm, and surface concentration of 13.17%. Thermochemical and burning rate values were assigned as described previously. These three profiles, along with one additional block profile, which was identified through IBHVG2 calculations to provide the same maximum chamber pressure as that of the ramp profile as well as corresponding performance values, are presented in figure 1. The block profile pressure match required a 0.036-mm deterrent penetration depth, with a surface concentration of 12.03% and exhibited a slight reduction (1.6%) in muzzle velocity when compared to predicted ramp profile ballistics.

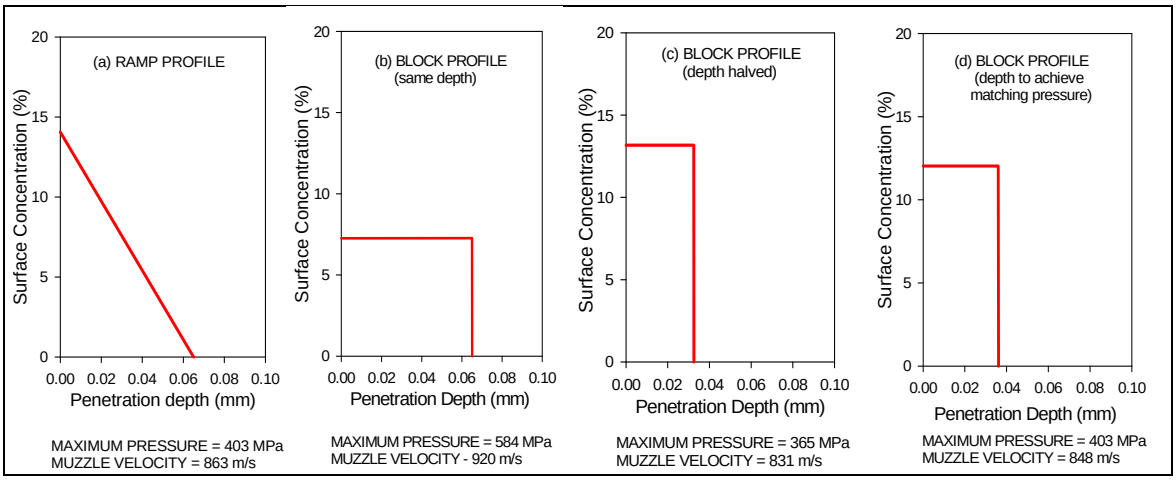

Figure 1. Deterrent concentration profiles and corresponding predicted performance for spherical ball propellant in a 5.56-mm gun.

Predicted chamber pressure and projectile velocity vs. time profiles using the previously mentioned data in the IBHVG2 code are shown in figure 2. Note the expected results of a higher initial pressurization rate with the block profile and its lower deterrent concentration at the surface but a slightly broader overall profile associated with the continuously increasing burning rate of the ramp profile. The ramp profile thus leads to peak pressure occurring at a later time and at a greater projectile displacement, resulting in about a 1% increase in piezometric efficiency and the muzzle velocity improvement mentioned previously.

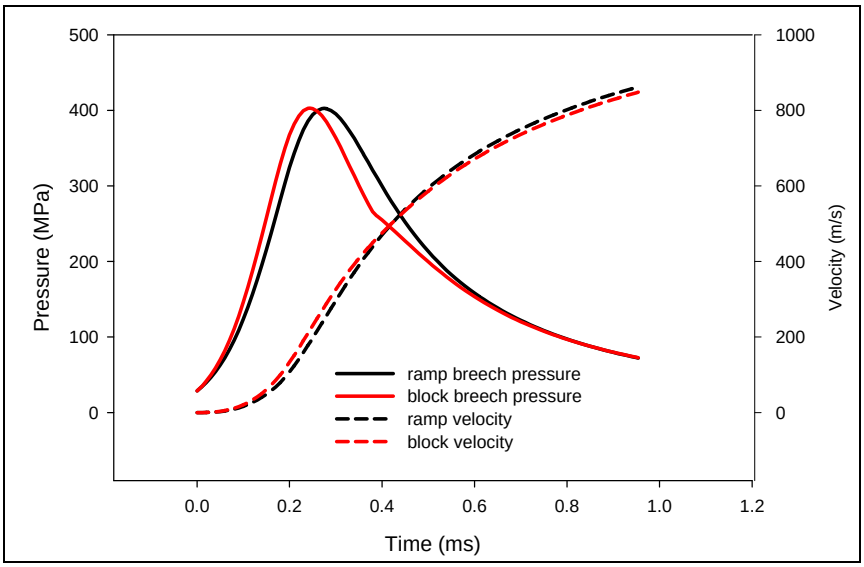

Figure 2. IBHVG2 ballistics predictions for spherical ball propellant in a 5.56-mm gun.

4. Computational Results – IBHVG2 Code/Oblate Spherical Propellant

A second series of calculations were performed using the IBHVG2 code addressing the oblate spherical geometry, an approximation of the geometry resulting from the "rolled ball" propellant process. IBHVG2 assumes the balls are flattened such that there exists two large flat circular surfaces of radius r_1 (i.e., top and bottom) connected by semispherical edges of radius r_2, maintaining an original volume described by a true sphere of radius r. (See the List of Symbols, Abbreviations, and Acronyms at the end of this report.)

Following the approach of the previous section, the grain surface as a function of burn distance was as follows:

$$S(x) = 2\pi r_1^{\,2} + 4\pi (r_2 - x)^2 , \tag{7}$$

or, using IBHVG2 terminology, where thickness $t = 2r_2$ and diameter $D = 2(r_1 + r_2)$,

$$S(x) = \pi D^2 / 2 - \pi Dt + 3\pi t^2 / 2 - 4\pi tx + 4\pi x^2 . \tag{8}$$

While equations 2 and 3 still apply to the new geometry, the total mass of deterrent was then expressed as follows:

$$m_d = \rho C_t \left[(4/3)\pi r_2^{\,3} + \pi r_1^{\,2} (2r_2) \right] = \rho C_t \pi \left(5t^3 / 12 - Dt^2 / 2 + D^2 t / 4 \right). \tag{9}$$

Substituting equations 8 and 9 into equations 2 and 3 and performing the required integrations and associated algebra, the equations relating penetration depth, surface concentration, and total concentration of deterrent for block and ramp profiles, respectively, became the following:

$$\begin{aligned} &\left(D^2/2 - Dt + 3t^2/2 \right) d_p - 2t d_p^{\,2} + 4 d_p^{\,3}/3 \\ &= \left(C_t / C_s \right) \left(5t^3/12 - Dt^2/2 + D^2 t/4 \right), \end{aligned} \tag{10}$$

and

$$\begin{aligned} &\left(D^2/4 - Dt/2 + 3t^2/4 \right) d_p - \left(2t/3 \right) d_p^{\,2} + d_p^{\,3}/3 \\ &= \left(C_t / C_s \right) \left(5t^3/12 - Dt^2/2 + D^2 t/4 \right). \end{aligned} \tag{11}$$

As before, these last two equations were used to generate concentration profiles and associated IBHVG2 input data files for a generic 30-mm gun, with charge parameters generally based on an M789 cartridge. At the 5% total deterrent concentration level, a 0.1-mm penetration depth yielded a 15.91% surface concentration for the ramp profile and 8.54% for the block profile. When the penetration depth was halved for the block profile, the surface concentration rose to 15.38%. A match to ramp profile performance was predicted to occur with a block penetration depth of 0.06 mm and a surface concentration of 13.10%, with a muzzle velocity loss of just under 1%. The four deterrent concentration profiles described are depicted in figure 3, along with corresponding performance predictions.

Figure 4 presents predicted chamber pressure and projectile velocity vs. time profiles resulting from the use of these data in IBHVG2. The resulting pressure-time profile for the block profile once again shows the expected higher initial pressurization rate; however, this time the transition at the depletion of the band of deterred propellant is readily visible, essentially similar to that seen with layered propellant (*2*). Nevertheless, the continuously increasing burning rate associated with the ramp profile yields a marginally higher muzzle velocity.

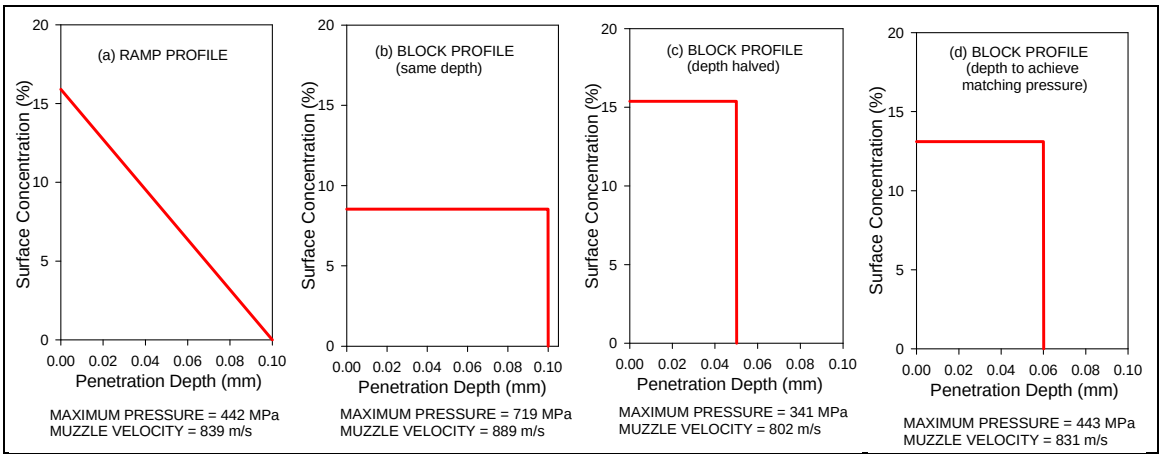

Figure 3. Deterrent concentration profiles and corresponding predicted performance for oblate spherical propellant in a 30-mm gun.

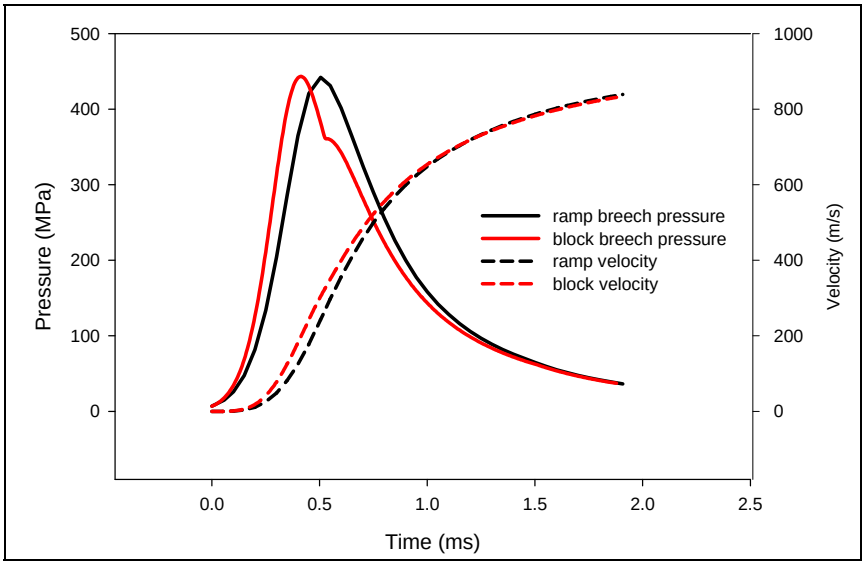

Figure 4. IBHVG2 ballistics predictions for oblate spherical propellant in a 30-mm gun.

5. Computational Results – IBHVG2 Code/Seven-Perforated Cylindrical Propellant

IBHVG2 computations were then performed to compare the predicted impact of ramp and block deterrent concentration profiles in seven-perforated cylindrical propellant grains, using a candidate 120-mm tank gun run as the subject. This propellant concept is of special interest

since it offers chemical and geometric progressivity for the gas generation rate as a function of burn distance into the grain, as first mentioned in the Background section (*5*).

The analysis follows as in prior sections, using nomenclature as defined in the List of Symbols, Abbreviations, and Acronyms at the end of this report. The grain surface as a function of burn distance became the following:

$$S(x) = 2\pi(R-x)(L-2x) + 14\pi(r+x)(L-2x) + 2\pi(r-x)^2 - 14\pi(r+x)^2 \ , \qquad (12)$$

and the total mass of deterrent

$$m_d = \rho C_t \pi\left(R^2 - 7r^2\right)L \ . \qquad (13)$$

As before, substituting equations 12 and 13 into equations 2 and 3 and performing the integration and considerable associated algebra, obtained the following equations relating penetration depth, surface concentration, and total deterrent concentration for the block and ramp profiles, respectively, as follows:

$$\begin{aligned} &-6d_p^{\,3} + \left(3L - 2R - 14r\right)d_p^{\,2} + \left(RL + 7rL + R^2 - 7r^2\right)d_p \\ &= \left(C_t / 2C_s\right)\left(R^2 - 7r^2\right)L, \end{aligned} \qquad (14)$$

and

$$\begin{aligned} &-3d_p^{\,3} + \left(2L - 4R/3 - 28r/3\right)d_p^{\,2} + \left(RL + 7rL + R^2 - 7r^2\right)d_p \\ &= \left(C_t / C_s\right)\left(R^2 - 7r^2\right)L \, . \end{aligned} \qquad (15)$$

Again, the last two equations were used to generate concentration profiles and associated IBHVG2 input data files for a nominal 120-mm cartridge. At a 5% total deterrent concentration level, a penetration depth of 0.73 mm yielded a surface concentration level of 20.62% for the ramp profile and 10.22% for the block profile. When the penetration depth was cut in half for the block profile, the surface concentration rose to 20.42%. A match in maximum pressure to the ramp profile prediction occurred at a penetration depth of 0.51 mm, with a corresponding surface concentration of 14.73%, with a velocity loss of about 0.8%. Figure 5 presents the four profiles and accompanying performance data.

Figure 6 presents predicted chamber pressure and projectile velocity vs. time profiles from IBHVG2 calculations employing the ramp and block (pressure match) profiles. Comments are similar to those from the preceding section: the block profile provides a higher initial pressurization rate and a clear demarcation of the transition from the deterred band to the core propellant composition (i.e., a profile characteristic of other layered propellant concepts).

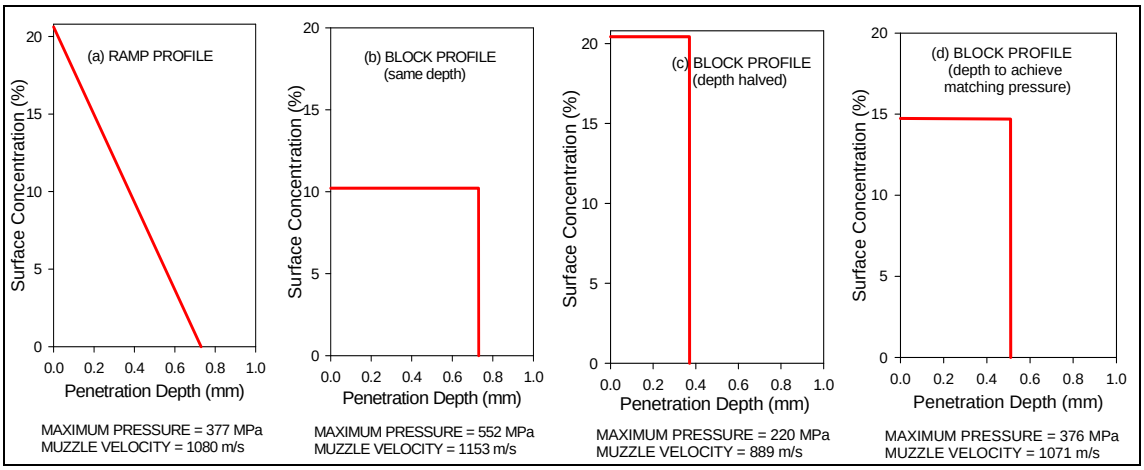

Figure 5. Deterrent concentration profiles and corresponding predicted performance for seven-perforated cylindrical propellant in a 120-mm gun.

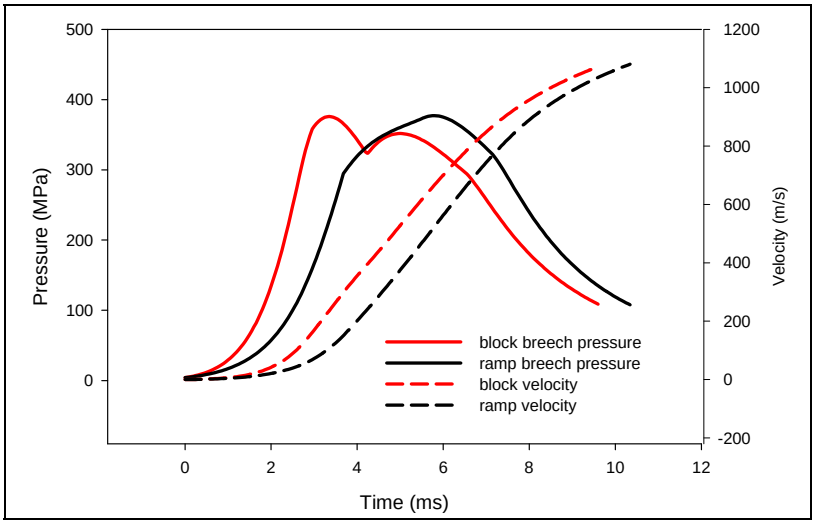

Figure 6. IBHVG2 ballistics predictions for seven-perforated cylindrical propellant in a 120-mm gun.

6. Computational Results – IBHVG2 Code/Seven-Perforated Cylindrical Propellant With No Deterrent in the Perforations

A final set of calculations employing the IBHVG2 codes addressed the same geometrical configuration (seven-perforated cylindrical) as in the previous section; however, this time, it was assumed that no deterrent was present on the internal surfaces (i.e., the walls of the seven perforations). Hence, the overall chemical contribution to the progressivity of gas generation from the deterrent was reduced; however, the higher initial burning rate within the perforations

provided for a slightly higher contribution to geometric progressivity, as the perforations (whose surfaces increased with burn distance) were regressing at a faster rate than the outer deterred surfaces (whose net surface decreased with burn distance). The overall effect was not intuitively obvious and may well be dependent on specific propellant parameters.

Following an analysis as just mentioned, the *initially deterred* outer surface as a function of burn distance was as follows:

$$S(x) = 2\pi(R - x)(L - 2x) + 2\pi(R - x)^2 - 14\pi(r + x)^2 . \qquad (16)$$

Equation 13 remained the correct expression for the total mass of deterrent, and equations 2 and 3 still applied. Performing the appropriate substitutions, integrations, and algebra one final time, the following equations were obtained relating penetration depth, surface concentration, and total deterrent concentration for the block and ramp profiles, respectively, as follows:

$$-8d_p^{\,3}/3 - (L + 4R + 14r)d_p^{\,2} + (2RL + 2R^2 - 14r^2)d_p = (C_t / C_s)(R^2 - 7r^2)L \ , \qquad (17)$$

and

$$-2d_p^{\,3} - (L + 4R + 14r)d_p^{\,2} + 3(RL + R^2 - 7r^2)d_p = (3C_t / C_s)(R^2 - 7r^2)L \ . \qquad (18)$$

One final time, the two equations were used to generate concentration profiles and associated IBHVG2 input data files, again for a nominal 120-mm cartridge. At a 5% total deterrent concentration level, a penetration depth of 0.80 mm yielded a surface concentration level of 28.17% for the ramp profile and 14.93% for the block profile. When the penetration depth was halved for the block profile, the surface concentration rose to 27.26%. A match in maximum pressure to the ramp profile prediction occurred at a penetration depth of 0.55 mm, with a corresponding surface concentration of 20.47%, yielding a velocity loss of about 2%. Figure 7 presents the four profiles and accompanying performance data.

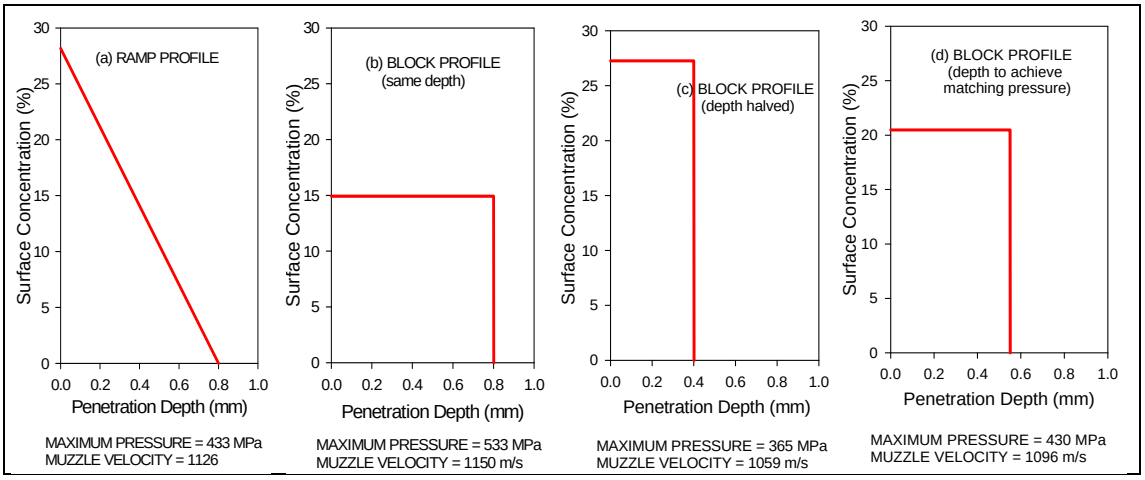

Figure 7. Deterrent concentration profiles and corresponding predicted performance for seven-perforated cylindrical propellant with no deterrent in the perforations, fired in a 120-mm gun.

Closing out this segment of the study, figure 8 presents predicted chamber pressure and projectile velocity vs. time profiles from IBHVG2 calculations employing the ramp and block (pressure match) profiles. While the block profile still provides a slightly higher initial pressurization rate, the lack of deterrent in the perforations mitigates this effect, and the transition from the deterred band to the core propellant composition is nearly unidentifiable in the pressure-time curve.

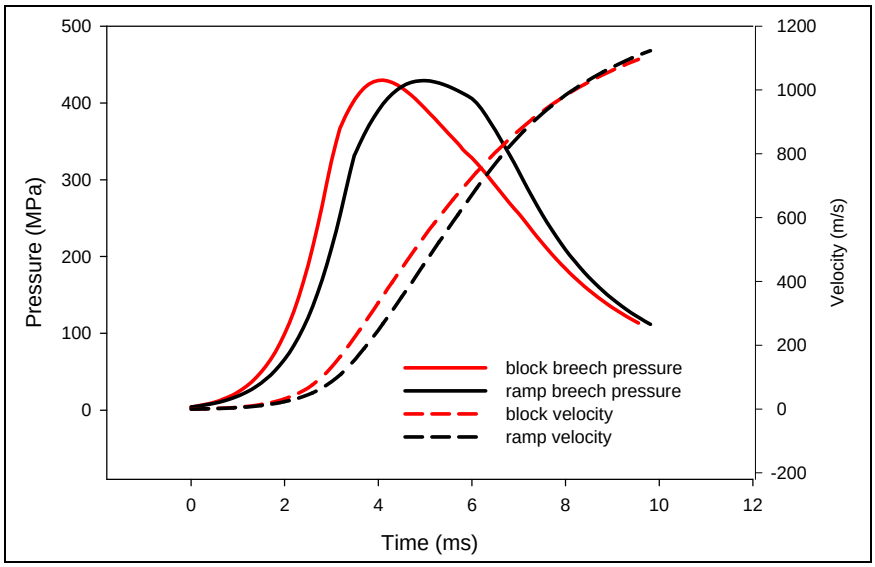

Figure 8. IBHVG2 ballistics predictions for seven-perforated cylindrical propellant with no deterrent in the perforations fired in a 120-mm gun.

7. Computational Results – XKTC Code/Spherical Ball Propellant

All of the previously described calculations employed the IBHVG2 interior ballistics code, and as described earlier in this report, this lumped-parameter analysis provides an excellent description of the interior ballistics cycle subject to assumptions such as uniform instantaneous ignition and subsequent combustion of the entire charge at a space-mean pressure throughout the chamber at each instant in time. Before drawing any final conclusions on the impact of deterrent representation on predicted performance and, by inference, actual deterrent distribution on actual gun performance, it seemed prudent to examine a couple of the previously mentioned propellant /gun configurations with a multiphase flow code to assess any impact on flame spreading and possible pressure waves.

The XKTC 1-D, with-area-change, two-phase flow code was employed to simulate the initial problem of spherical ball propellant in a 5.56-mm gun. Fortunately, the algorithms previously developed apply here and input data corresponding to that used in the IBHVG2 analysis was

appropriately transferred to XKTC (with some additional data required). In actuality, the XKTC calculations were run with three ignition conditions: uniform, instantaneous ignition; a slow base igniter profile (occurring over 2 ms); and a harsh base igniter profile (0.2-ms duration). Predicted breech pressure, forward pressure, and differential pressure vs. time for ramp and block deterrent concentration profiles and for each of the three ignition conditions are presented in figure 9.

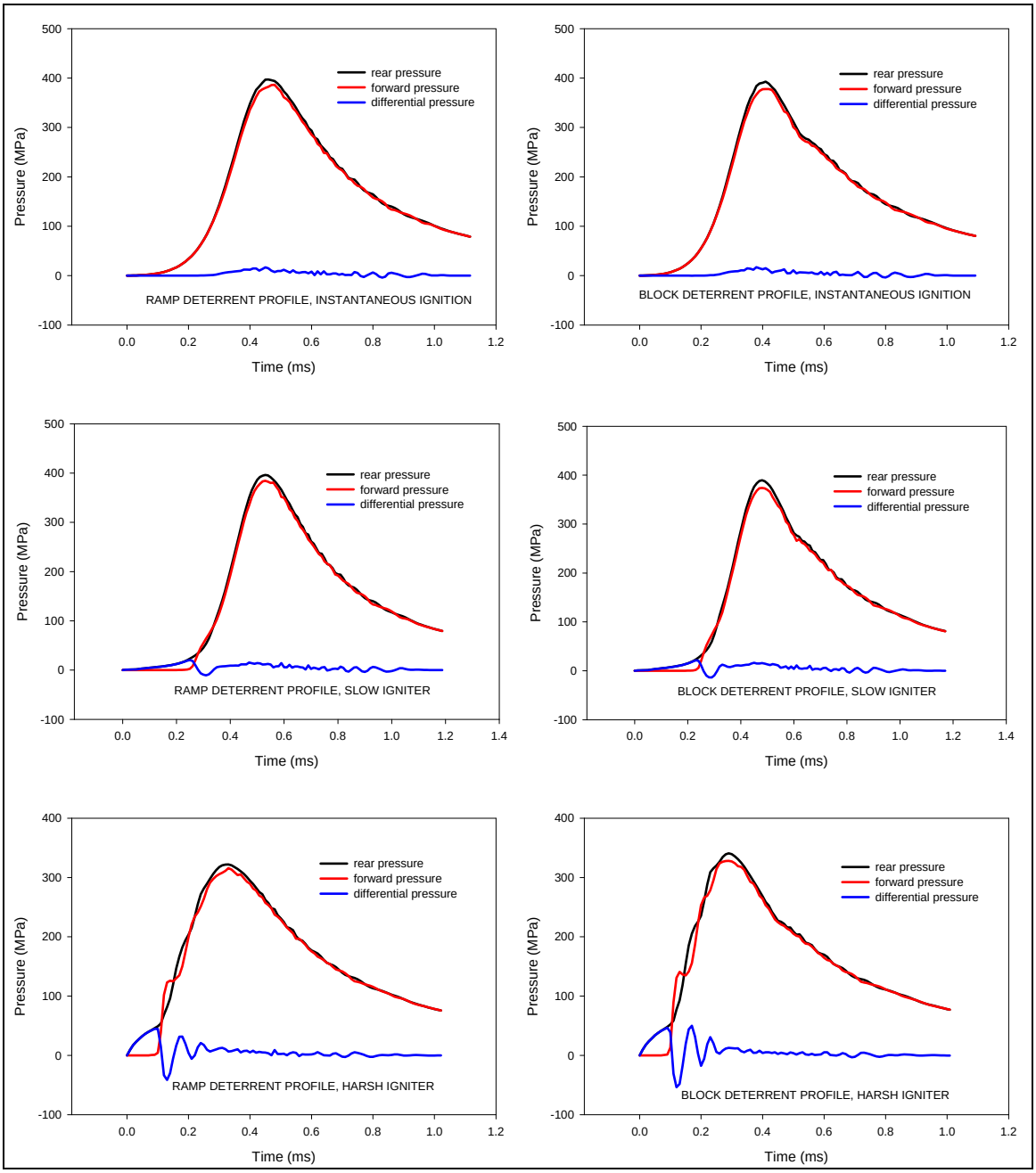

Figure 9. XKTC ballistics predictions for spherical ball propellant in a 5.56-mm gun with ramp and ball deterrent profiles with different igniters.

The results are quite interesting in that while they agree within 1% with those of the IBHVG2 predictions for the instantaneous ignition condition, a growing divergence is seen to accompany the severity of a localized ignition event and accompanying flow dynamics. Pressure waves increase and maximum chamber pressure and muzzle velocity drop. While the details of the interaction are likely quite complex and specifically dependent on propellant and igniter parameters, it appears that the programming of mass generation rate intended to result from the presence of the deterrent is complicated by (1) flame spreading rate and (2) local delays in ignition resulting from bed compaction at the base of the projectile caused by the strong pressure wave at the leading edge of the combustion front. The clear implication is that some interplay exists between optimization of deterrent profile and the ignition process (including igniter design and propellant bed permeability and mechanical properties).

8. Computational Results – XKTC Code/Seven-Perforated Cylindrical Propellant

A second pair of calculations using the XKTC code were performed on the seven-perforated cylindrical propellant example (all surfaces deterred) previously run using IBHVG2. This time, a realistic, though idealized, igniter profile was employed rather than an assumption of instantaneous ignition of all propellant surfaces. Nevertheless, the results from both codes were quite comparable, with maximum pressures and muzzle velocities each within 1%. Moreover, figure 10 displays ballistics predictions of pressure-time curves and projectile in-bore velocity profiles, which appear qualitatively quite similar to those of figure 6. Other than some very minor inflections in the pressure curves, likely a consequence of the influence of flame spread on ensuing two-phase flow, no additional significant features are revealed using the multiphase flow XKTC code. This one set of calculations does not, of course, ensure that unknown pathologies might not accompany untried extreme ignition profiles, again, outside the scope of the lumped-parameter code.

Note that on direct comparison of IBHVG2 and XKTC, results for the 120-mm gun reveal one distinct feature worthy of mention. Figure 11 provides an overlay of the two sets of results. While a general delay in the onset of pressurization is expected to accompany the period of flame spread treated in XKTC but assumed to be instantaneous in IBHVG2, overall pressurization rates between block and ramp profiles are seen to be quite different for the two codes. Since the same primer output profile was used for propellants with block and ramp profiles, one must consider the role of pressurization during flame spread due to very early combustion of newly ignited propellant. The growth in disparity (nearly 1 ms additional delay at 200 MPa) using XKTC might well be a consequence of the fact that a convectively driven flame spread, driven by the primer output and the early combustion products, will be faster for the block profile propellant because of its lower surface deterrent concentration and, hence, initial burning rates.

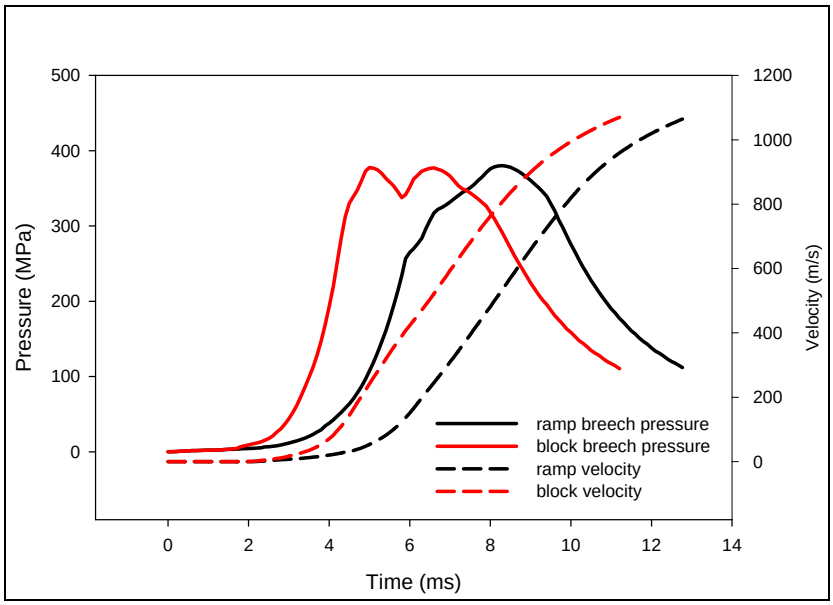

Figure 10. XKTC ballistics predictions for seven-perforated cylindrical propellant (all surfaces deterred) in a 120-mm gun.

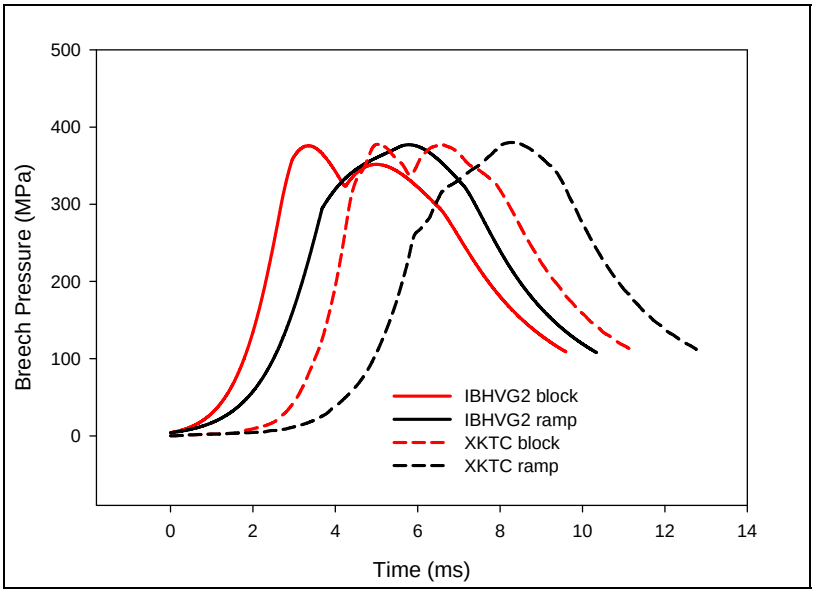

Figure 11. Comparison of IBHVG2 and XKTC ballistic predictions for seven-perforated cylindrical propellant (all surfaces deterred) in a 120-mm gun.

To examine this hypothesis, we have plotted the histories of flame spread predicted by XKTC for the two propellants (figure 12). Recalling that XKTC is a 1-D code and flame spread takes place in the axial direction only (i.e., no radial convection takes place to ignite immediately the propellant adjacent to the primer tube), the qualitative nature of these results is as expected. The region of primer efflux is easily identified, with initial propellant ignition taking place at the two ends of this region and subsequently proceeding both to the extreme ends of the chamber and inwards to the region of primer venting itself. As expected, the times of initial ignition are the same for both propellants, but then very rapidly the flame front in the propellant with the block deterrent profile propagates throughout the chamber at a substantially greater rate, with completion occurring about a millisecond sooner than for the propellant with the ramp deterrent profile. These results appear to confirm our hypothesis; multidimensional simulations of flame spreading should add even more insight to the process.

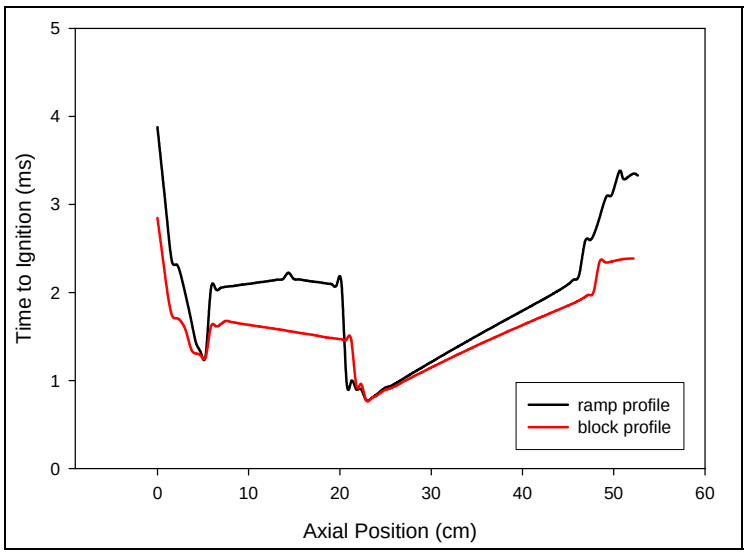

Figure 12. XKTC predictions of flame spread for seven-perforated cylindrical propellant (all surfaces deterred) in a 120-mm gun.

9. Computational Results – NGEN Code/Seven-Perforated Cylindrical Propellant

Finally, the NGEN multidimensional, multiphase flow interior ballistics code was employed to investigate the influence of deterrent profile representation on predicted ballistics results for the seven-perforated cylindrical propellant (all surfaces deterred) fired in a 120-mm gun. This time, the possibility of radial as well as axial flame spread and ensuing gas- and solid-phase flow was allowed.

Figure 13 shows a schematic of the computational domain used in the NGEN code for the current simulation of the 120-mm gun. Note the figure has the ordinate magnified by about a factor of 6 for clarity. In the axial direction, the domain extends from the breech face (X = 0) to the base of the projectile at 54.1 cm (i.e., defined for the present application as the location on the projectile where the diameter matches that of the launch tube); because an axisymmetric configuration is assumed in this case, the domain extends in the radial direction from the chamber centerline (Y = 0) to the radial wall of the chamber (7.715 cm). The projectile afterbody extends 27.3 cm behind the projectile base and into the gun chamber; the fin set, which in practice is positioned on the projectile tailboom, is excluded. The black, green, and purple "dots" located on the radial tube wall mark the axial locations from the breech face (1, 25, and 40 cm) at which wall pressure values are collected as a function of time (see discussion for figures 14 and 15).

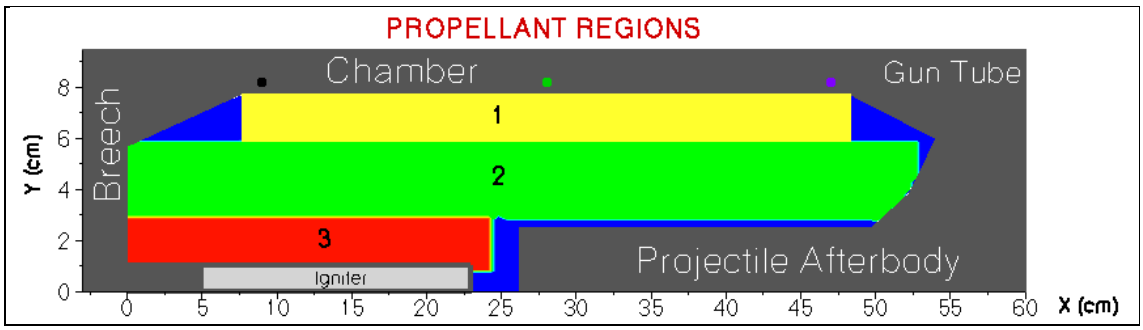

Figure 13. Representation of solid propellant regions used in the NGEN code (see text for description).

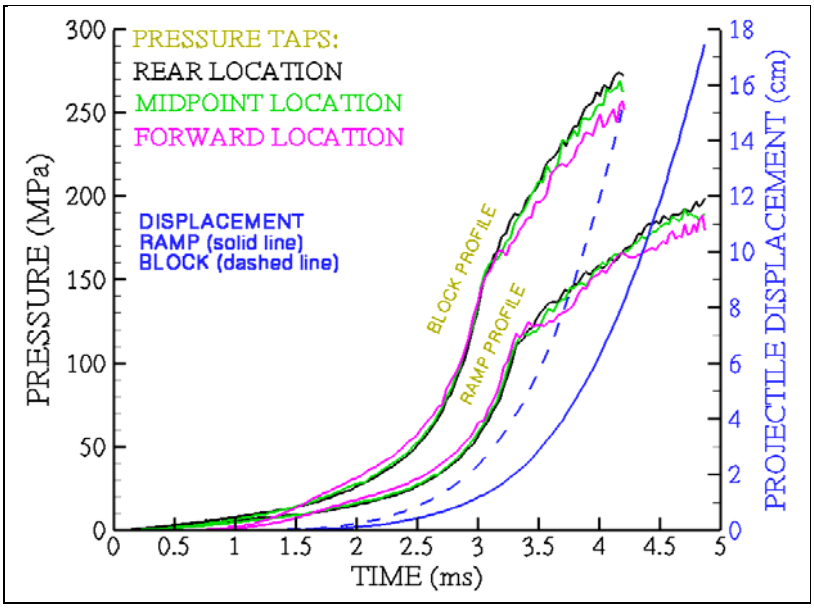

Figure 14. Chamber wall pressures at three locations (NGEN code) and projectile displacement for seven-perforated cylindrical propellant in a 120-mm gun – to 5 ms.

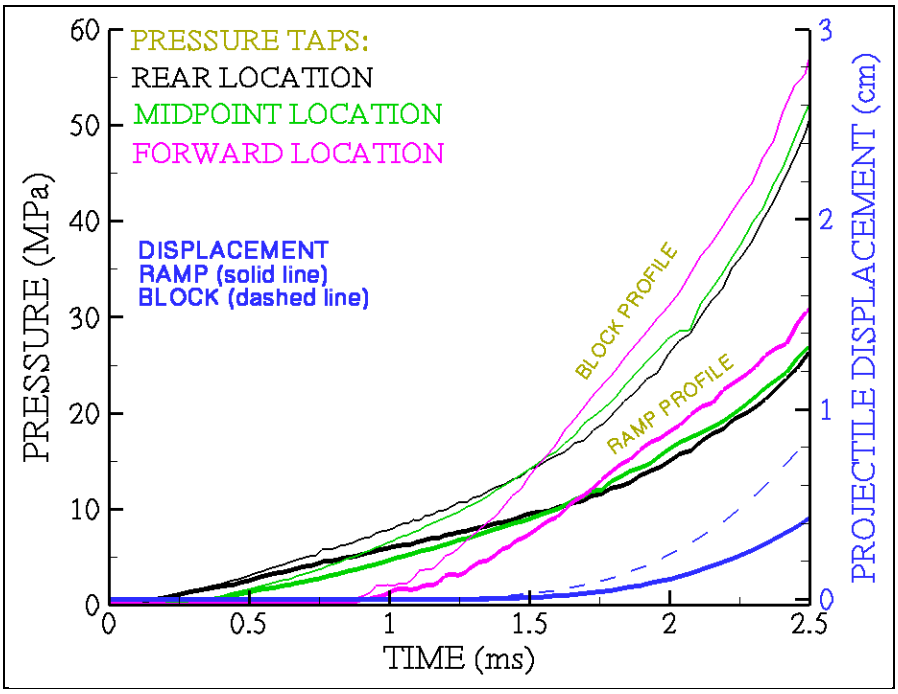

Figure 15. Chamber wall pressures at three locations (NGEN code) and projectile displacement for seven-perforated cylindrical propellant in a 120-mm gun – to 2.5 ms.

The three propellant regions (denoted 1, 2, and 3 in figure 13) were chosen to represent as closely as possible a reasonable loading of the chamber that also accounts for regions of ullage beneath the chambrage, at the base of the projectile, and along the projectile afterbody while, at the same time, yielding a settling porosity of about 0.4 throughout. Each region contains a quantity of seven-perforated deterred propellant that together totals 7750 g. Charge combustion in region 3 is started by the centercore igniter (diameter of 2 cm), extending from 5 to 23 cm from the breech face and is implicitly represented by a region that generates a hot Benite gas flux (206 g/cm^3/s) over a time period of 0 to 2 ms. An additional igniter mechanism of this type is used to represent the combustible case that radially envelopes all of the solid propellant regions and generates a hot gas flux of 2 g/cm^3/s over a time period from 3.5 to 10 ms.

Figure 16 shows the computed pressures as a function of time over the breech face and projectile base (spatial averages). The results for the ramp and block propellant deterrent profiles are shown. As seen in figure 10 (XKTC code results), the pressure rise is faster for the block profile. Evidence of pressure waves (i.e., pressure reversals between the breech and the base) is clear for times earlier than about 3 ms. Comparing figures 10 and 16, the block profile results are quite similar (pressure of about 250 MPa at 4 ms), while the ramp profile produces higher pressures (about 150 MPa) at 4 ms using the NGEN code simulation than for the XKTC code simulation (about 50 MPa). This effect is the result of both radial flame spreading and the presence of radial ullage in the NGEN code results (recall figure 13).

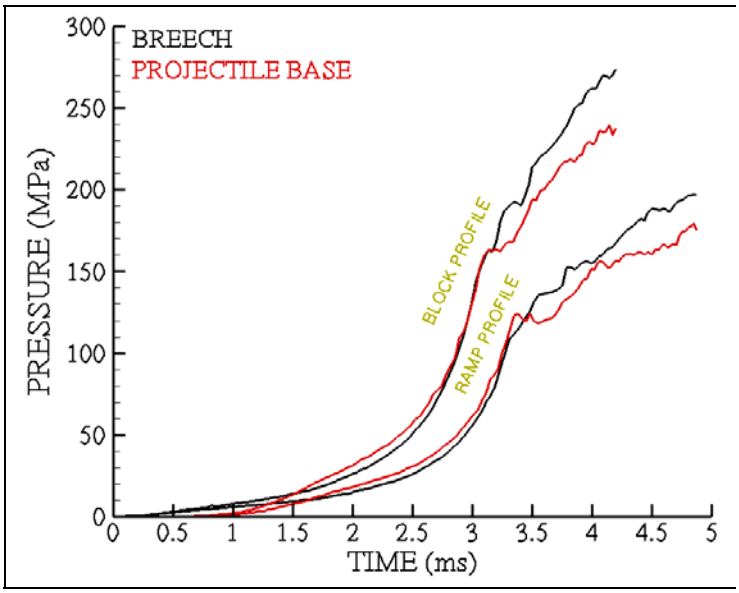

Figure 16. Breech and projectile base pressures (NGEN code) for seven-perforated cylindrical propellant in a 120-mm gun.

Figures 14 and 15 show pressure results for three locations along the radial wall of the chamber as well as the projectile displacement for about 5 ms of the simulations. These results serve to amplify those of figure 16 (i.e., accelerated flame spreading of the block-profile deterred propellant and the presence of axial pressure wave activity for both cases) but also indicate that, as expected, the projectile is displaced faster for the charge that employs block-profile deterred propellant. In addition, these results indicate the possible presence of radial pressure waves (oscillations) in the chamber after about 3 ms when projectile displacement is significant. Indeed, NGEN code simulations rerun with finer radial grids support the presence of these low-amplitude and low-frequency waves. It should be noted the discontinuity in the pressure-time curves at 3.5 ms as displayed in figures 14–16 is due to the initiation of the combustible case when the charge is fully ignited in the radial extreme.

The detailed results of the NGEN code simulation are displayed in figures 17–24 for times of 0.3–4.2 ms from start of outflow from the igniter (recall figure 13). Note each figure has the ordinate magnified by about a factor of 6 for clarity. During this time period, the ignition and flame spreading are prominent. After 2 ms, the projectile begins travel down the tube (recall figures 14 and 15). Modeling results are not presented in this report for times greater than 4.2 ms for brevity. In each figure, results at a particular time are displayed using color contours of three computed variables—propellant bed porosity, propellant temperature, and gas pressure. Velocity vectors (in white) are overlaid in each case displaying the magnitude (via vector length) and direction of the local gas field. The porosity (plotted with limits of 0–1: red and blue) of the

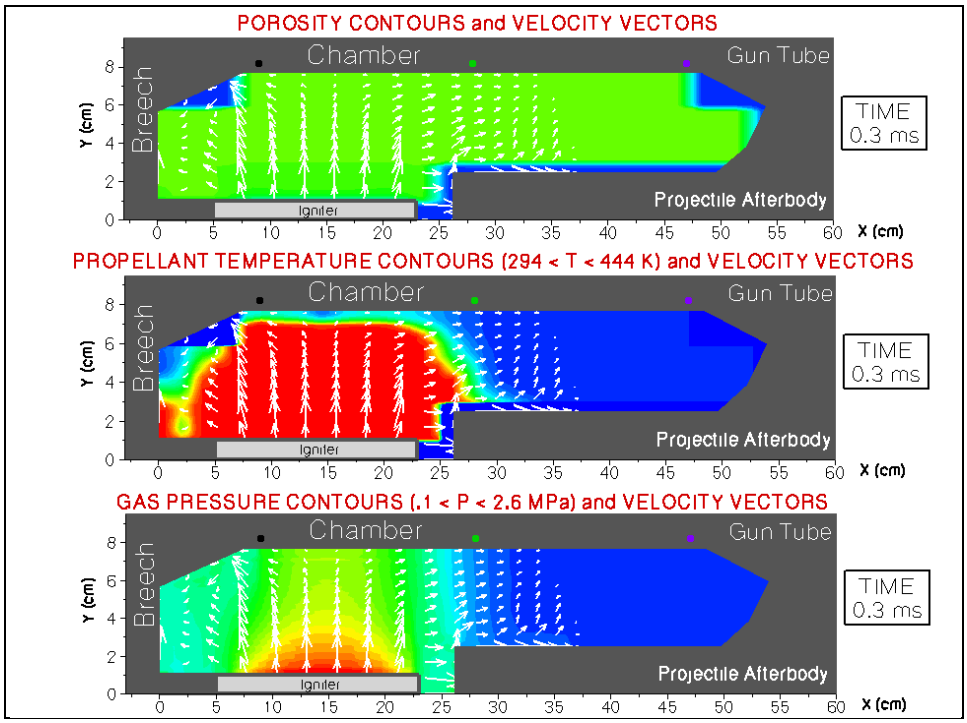

Figure 17. Flow velocity vectors and color contours (NGEN code) of porosity, propellant temperature, and gas pressure for seven-perforated cylindrical propellant in a 120-mm gun at 0.3 ms using the ramp deterrent profile.

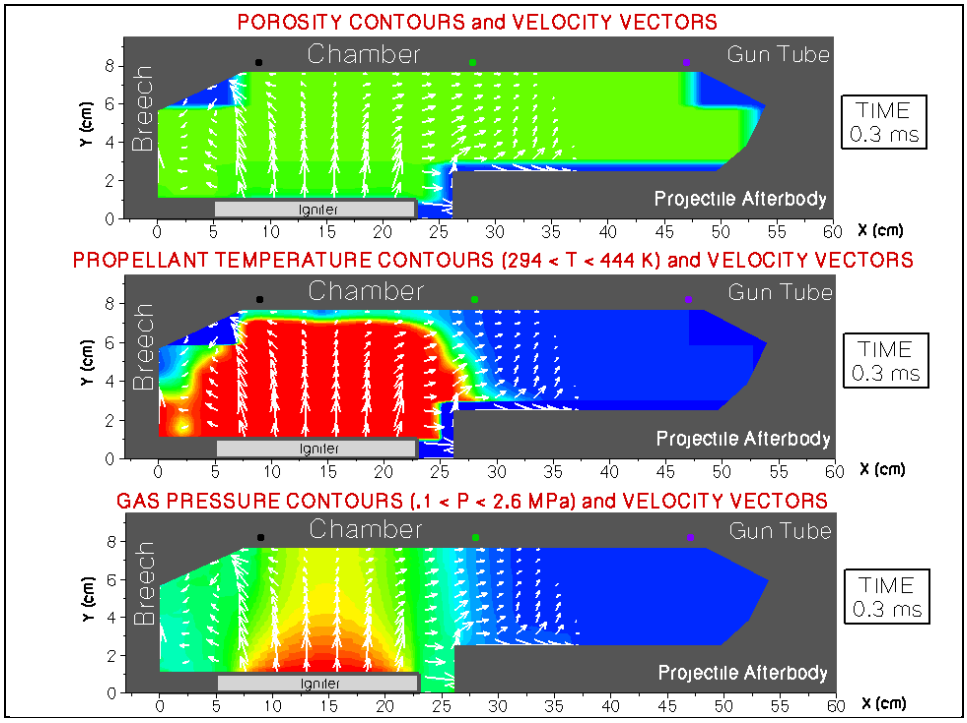

Figure 18. Using the block deterrent profile.

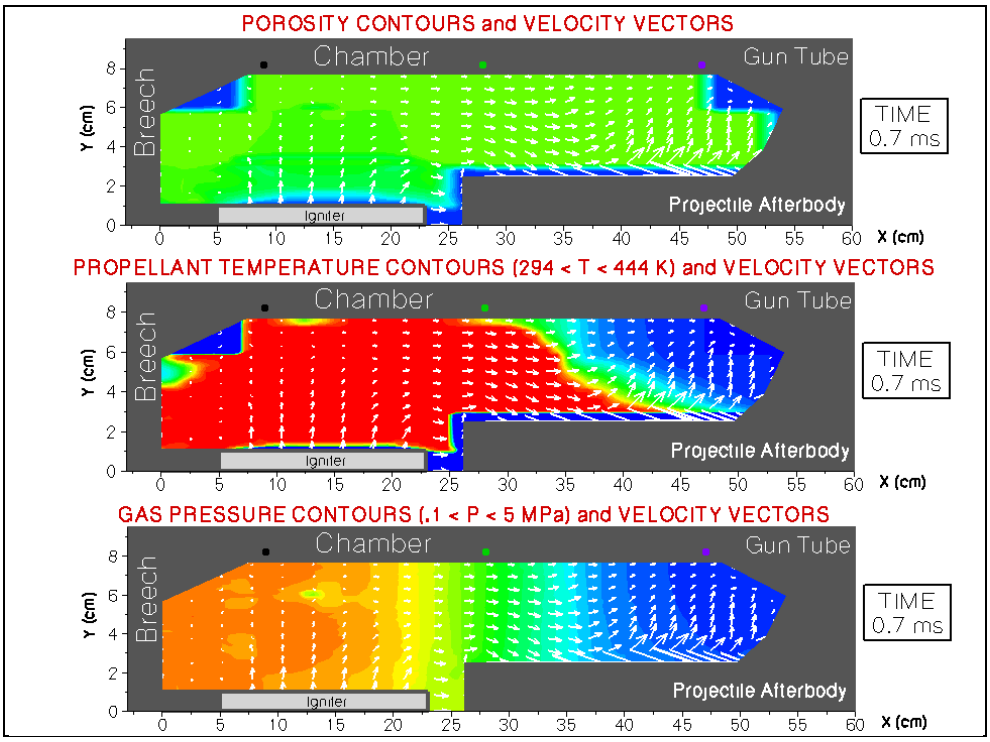

Figure 19. Flow velocity vectors and color contours (NGEN code) of porosity, propellant temperature, and gas pressure for seven-perforated cylindrical propellant in a 120-mm gun at 0.7 ms using the ramp deterrent profile.

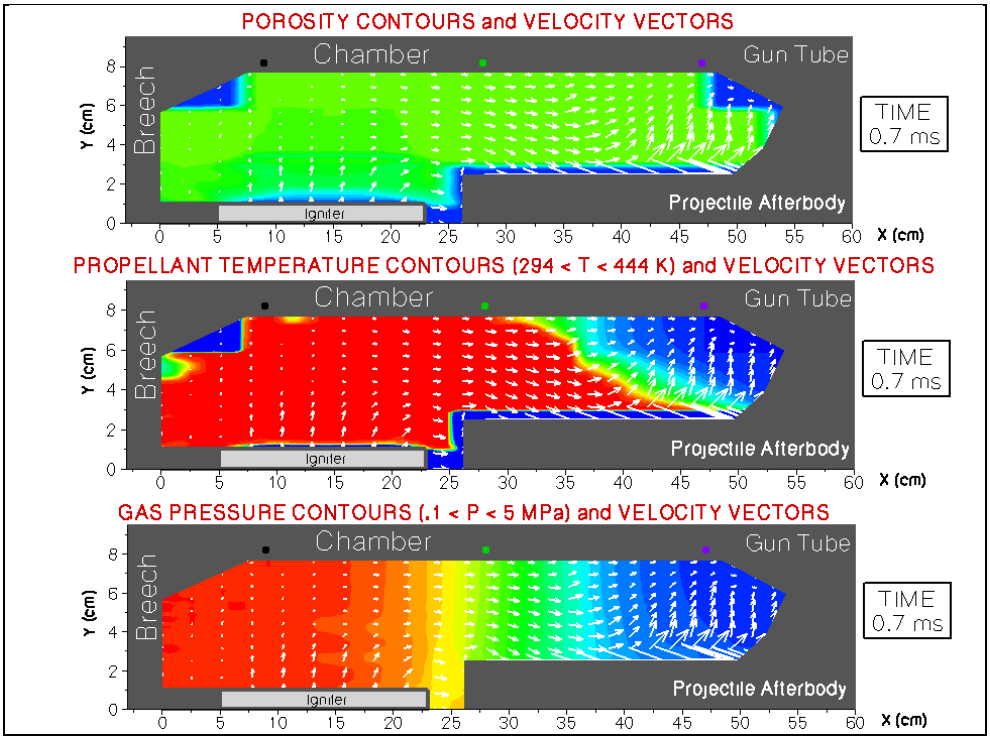

Figure 20. Using the block deterrent profile.

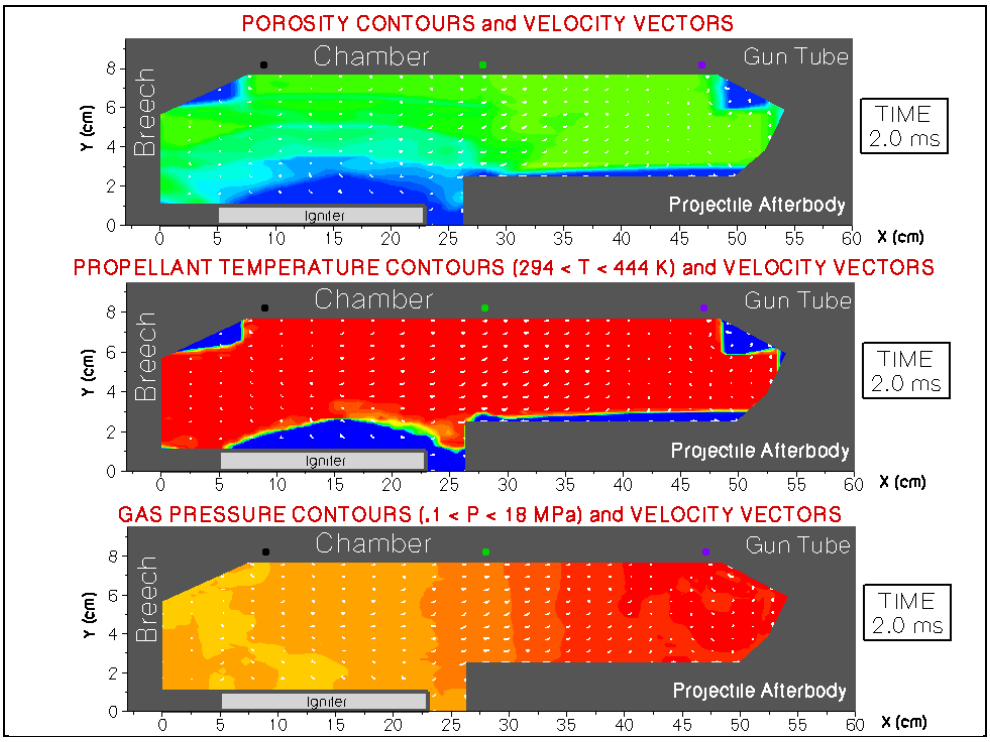

Figure 21. Flow velocity vectors and color contours (NGEN code) of porosity, propellant temperature, and gas pressure for seven-perforated cylindrical propellant in a 120-mm gun at 2.0 ms using the ramp deterrent profile.

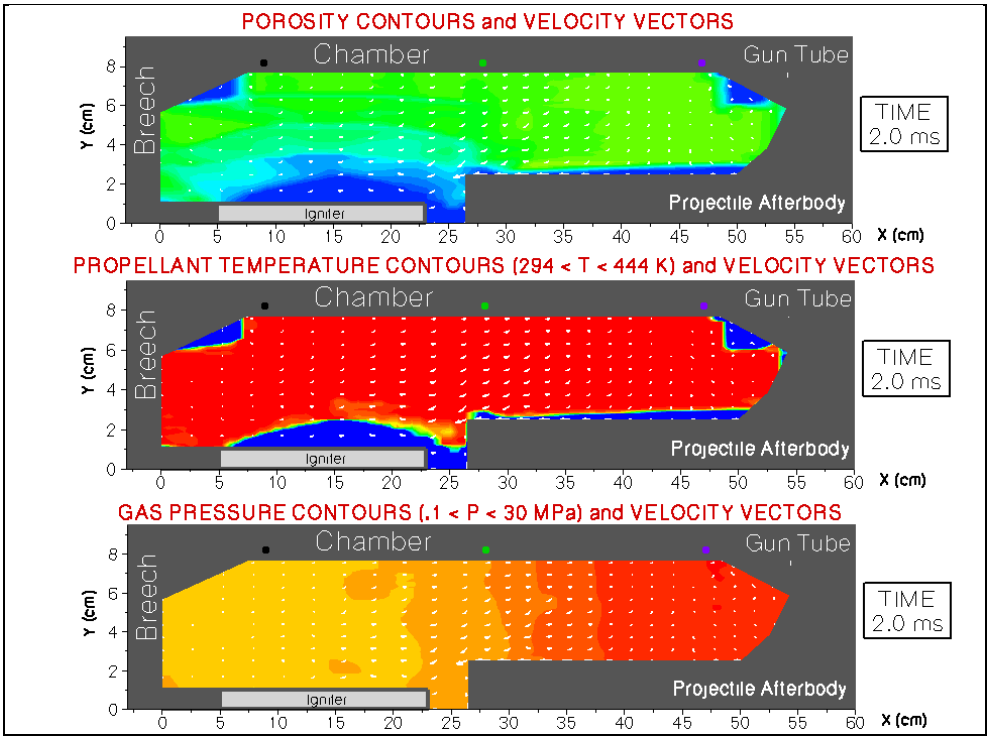

Figure 22. Using the block deterrent profile.

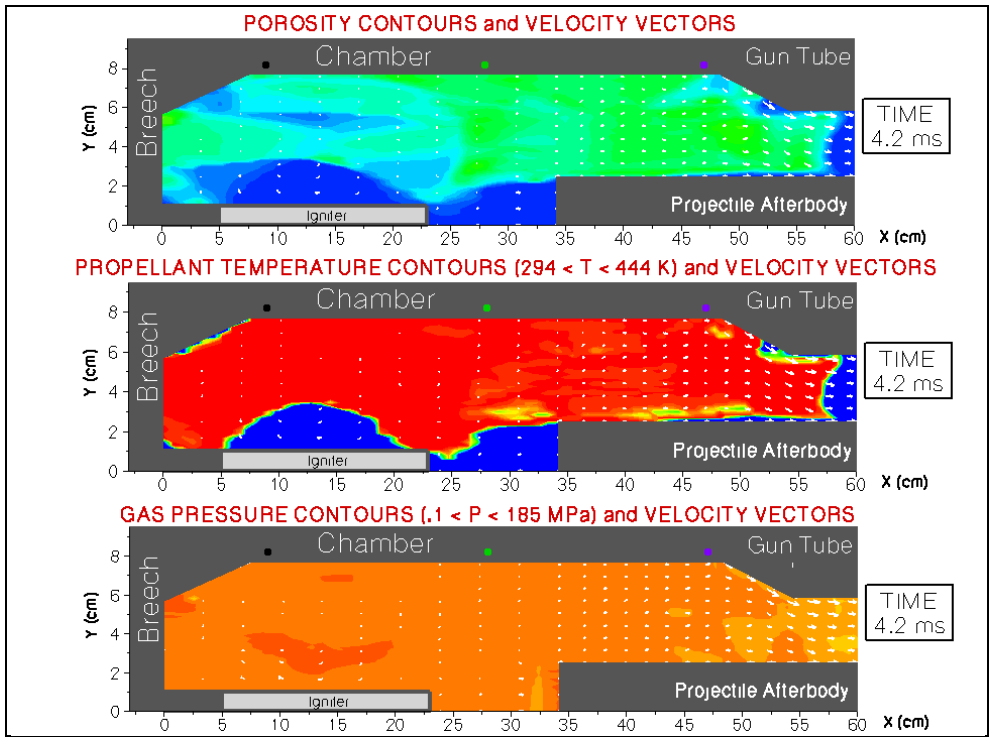

Figure 23. Flow velocity vectors and color contours (NGEN code) of porosity, propellant temperature, and gas pressure for seven-perforated cylindrical propellant in a 120-mm gun at 4.2 ms using the ramp deterrent profile.

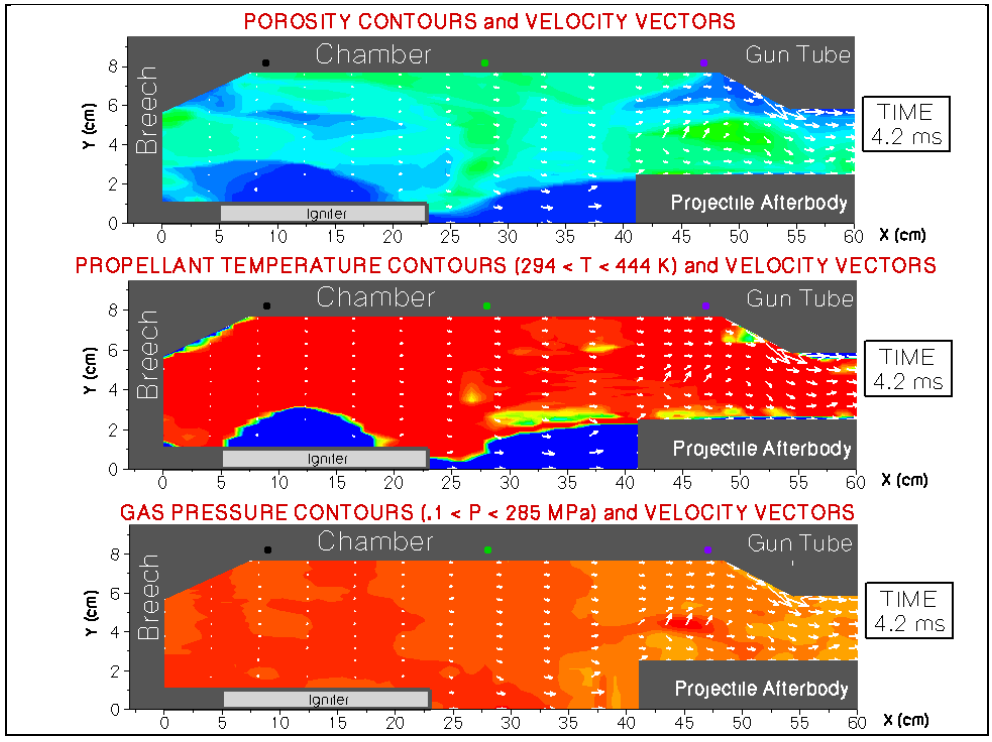

Figure 24. Using the block deterrent profile.

entire propellant bed is initially about 0.4 (green); the displacement and consumption of propellant is indicated by a color change to light blue. The location of ignited propellant is indicated by colors from green to red (i.e., warm to ignition temperature of 444 K). High gas pressure is indicated by the color red, with lower pressures indicated by a succession of colors from orange to blue (note that plotted pressure limits change with each figure).

Figures 17 and 18 show that at 0.3 ms, flame spreading, which is chiefly radial, has progressed to about one-half of the charge, although high gas pressure (2.6 MPa and above) is only evident near the active igniter. Gas flow through the propellant regions is already indicating some regions of two-dimensional structure. Comparing figures 17 and 18, it can be noted that even at this early time, the propellant using the block-profile deterrent is slightly more advanced in flame spreading.

Figures 19 and 20 show that at 0.7 ms, the charge is about 70% ignited, gas flow has permeated the entire bed, and gas pressures in the chamber are notably higher for the propellant using the block profile for deterrent (note the consistent pressure scale used for figures 19 and 20).

Figures 21 and 22 show that at 2 ms, the entire propellant charge is flame spread and some propellant in region 1 has already been consumed. The presence of a pressure reversal is evident from the higher gas pressures at the projectile base for both cases, although it has become necessary to use an elevated scale for the gas pressure contours of the block-profile deterred propellant (i.e., the color red indicates 30 MPa and above for the block results, compared to 18 MPa for the ramp results).

Figures 23 and 24 show that at 4.2 ms, the charge is being consumed at a more rapid rate (the combustible case was ignited at 3.5 ms, when the charge was fully flame spread in the radial extreme) and that displacement of the projectile is significant due to the high gas pressures in the chamber—much higher for the propellant that uses the block-profile deterrent (figure 24). In each case, burning propellant is being drawn into the gun tube behind the advancing projectile. Overall, the color contour plots of the computed results using the NGEN code support the pressure-time results and add an additional dimension to the analysis of this charge. It is clear that both axial and radial flame spreading are more advanced for the propellant utilizing the block-profile for the deterrent layer, despite the introduction of regions of radial ullage into the charge modeled using the NGEN code.

10. Discussion

Calculations were performed using two different deterrent concentration profiles in four propellant types using three levels of interior ballistics codes. Lumped-parameter simulations using the IBHVG2 code demonstrated that, assuming a given value for the total deterrent

concentration within the overall propellant composition, nearly identical ballistics results (maximum chamber pressure and projectile muzzle velocity) can be obtained using either ramp or block deterrent concentration profiles with some adjustment in the assumed deterrent penetration depth and a corresponding correction in the surface concentration. Depending on which two of these parameters are actually known, the algorithms reported previously allow assignment of a hypothetical profile with the third quantity defined. While full experimental characterization of the deterrent concentration and profile is irreplaceable, reasonable predictions of interior ballistics performance can be made using this technique. Note, however, that the details of the pressure-time curve, and hence the in-bore acceleration profile, will depend on the profile shape employed—the unlikely block deterrent concentration profile essentially mimicking a layered propellant concept. Incidentally, while it is noted that the ramp profile predictions always gave a marginally higher muzzle velocity for the same maximum pressure than did those for the block profile, it should be pointed out that the propellant characteristics associated with the surface and core positions in this propellant were not those optimized for layered propellants. One should not generalize these results with respect to the performance potential of layered propellant concepts in general.

Having made these somewhat optimistic comments based on the lumped-parameter results, the XKTC simulations motivate a word of caution with respect to any apparently benign nature of the profile representation. A sensitivity of even gross gun performance to profile representation, under localized ignition conditions, demonstrates the influence of the differing initial burning rates associated with the different deterrent surface concentrations. Whether this effect is merely a concern to the modeler or actually offers an exploitable feature to the propellant developer is largely dependent on their ability to characterize and control the profile during production. Further, flame-spreading rates are shown, even in this 1-D representation, to depend on deterrent profile as well as primer output. The added fidelity of the multidimensional simulations offered by NGEN serves to further discriminate the impact of the deterrent profile representation. While the charge configurations studied in this report were not only axisymmetric but also essentially full bore (no substantial circumferential ullage external to the charge to complicate the path of flame spreading and pressurization, as typical for artillery charges), more complex geometries would likely yield more significant differences using a multidimensional representation.

11. Concluding Remarks

The study described herein quantifies the influence of two hypothetical (but relevant) deterrent concentration profiles on the predicted performance of several common propellant grain configurations with deterred surfaces. While systems modeled are generic and some of the

propellant characteristics arbitrarily chosen, this study documents results associated with commonly used simple profiles. These simple representations allow definition of self-consistent values for the primary deterrent parameters (i.e., total quantity, surface concentration, and penetration depth); however, discrepancies from reality in propellant surface burning rates lead, on the classical level, to corresponding discrepancies in pressurization and projectile acceleration. On a more phenomenologically detailed level, the interplay of these rates with flame spread, the formation of pressure waves, and bed stresses and compaction offers a potential for either exploitable or deleterious effects—once again, underscoring the need for use of not only the best possible codes, but equally important, the best possible input data.

12. References

1. Levy, M. E. *The Use of Deterrents in Small Arms Propellants: A Comprehensive Review*; FA-TR-76004; Frankford Arsenal: Philadelphia, PA, April 1976.
2. Horst, A. W. *A Brief Journey Through the History of Gun Propulsion*; ARL-TR-3671; U.S. Army Research Laboratory: Aberdeen Proving Ground, MD, November 2005.
3. Lawhon, J.; Drummond, J.; O'Meara, W.; Pulver, R. Hybrid Propellant for Small, Medium, and Large Caliber Applications. *Proceedings of the NDIA Guns and Ammunition, Missiles, and Rockets Conference and Exhibition*, Baltimore, MD, April 2004.
4. Freedman, E. *BLAKE – A Thermodynamics Code Based on TIGER: Users' Guide to the Revised Program*; ARL-CR-422; U.S. Army Research Laboratory: Aberdeen Proving Ground, MD, July 1998.
5. Anderson, R. D.; Fickie, K. D. *IBHVG2 – A User's Guide*; BRL-TR-2829; U.S. Army Ballistics Research Laboratory: Aberdeen Proving Ground, MD, July 1987.
6. Gough, P. S. *Interior Ballistics Modeling: Extensions to the XKTC Code and Analytical Studies of Pressure Gradient for Lumped Parameter Codes*; ARL-CR-460; U.S. Army Research Laboratory: Aberdeen Proving Ground, MD, February 2001.
7. Gough, P. S. Modeling Arbitrarily Packaged Multi-Increment Solid Propellant Charges of Various Propellant Configurations. *Proceedings of the 33rd JANNAF Combustion Meeting*, November 1996, CPIA Publication 653, Vol. 1, pp 421–435.
8. Gough, P. S. *Extensions to the NGEN Code: Propellant Rheology and Container Properties*, October 1997, CPIA Publication 662, Vol. 3, pp 265–281.
9. Nusca, M. J.; Gough, P. S. Numerical Model of Multiphase Flows Applied to Solid Propellant Combustion in Gun Systems. *Proceedings of the 36th Aerospace Sciences Meeting*, American Institute of Aeronautics and Astronautics, AIAA Paper No. 1998–3695, July 1998.
10. Nusca, M. J. *High-Performance Computing and Simulation for Advanced Armament Propulsion*; ARL-TR-3215; U.S. Army Research Laboratory: Aberdeen Proving Ground, MD, June 2004.
11. Boris, J. P.; Landsburg, A. M.; Oran, E. S.; Gardner, J. H. *LCPFCT – A Flux-Corrected Transport Algorithm for Solving Generalized Continuity Equations*; NRL-MR/6410-93-7192; U.S. Naval Research Laboratory: Washington, DC, April 1993.
12. Horst, A. W.; Conroy, P. C. *Flame-Spreading Processes in a Small-Caliber Gun*; ARL-TR-4181; U.S. Army Research Laboratory: Aberdeen Proving Ground, MD, July 2007.

List of Symbols, Abbreviations, and Acronyms

Common Nomenclature

C_s deterrent concentration at the grain surface

C_t average deterrent concentration within the grain

d_p depth of penetration of the deterrent into the grain

m_d total mass of deterrent in a grain

S instantaneous total surface of a grain

x distance burned into the grain

ρ density of propellant (assumed constant within grain)

Nomenclature Unique to Spherical Grain

r initial radius of spherical grain

Nomenclature Unique to Oblate Spherical Grain

r_1 initial radius of flat round top and bottom surfaces of oblate spherical grain

r_2 initial radius of semispherical edges of oblate spherical grain

D $2(r_1+r_2)$, major diameter of oblate spherical grain, as used in IBHVG2

t $2r_2$, thickness of oblate spherical grain, as used in IBHVG2

Nomenclature Unique to Cylindrical Grains

L length of cylindrical grain

R radius of cylindrical grain

r radius of perforation in cylindrical grain

NO. OF
COPIES ORGANIZATION

1 (PDF only) DEFENSE TECHNICAL INFORMATION CTR
DTIC OCA
8725 JOHN J KINGMAN RD
STE 0944
FORT BELVOIR VA 22060-6218

1 DIRECTOR
US ARMY RESEARCH LAB
IMNE ALC HR
2800 POWDER MILL RD
ADELPHI MD 20783-1197

1 DIRECTOR
US ARMY RESEARCH LAB
AMSRD ARL CI OK TL
2800 POWDER MILL RD
ADELPHI MD 20783-1197

1 DIRECTOR
US ARMY RESEARCH LAB
AMSRD ARL CI OK PE
2800 POWDER MILL RD
ADELPHI MD 20783-1197

ABERDEEN PROVING GROUND

1 DIR USARL
AMSRD ARL CI OK TP (BLDG 4600)

NO. OF COPIES ORGANIZATION

3 DIRECTOR
US ARMY RESEARCH LAB
AMSRD ARL RO P
D MANN
R ANTHENIEN
TECH LIB
PO BOX 12211
RESEARCH TRIANGLE PARK NC
27709-2211

8 US ARMY AVIATN & MSLE CMMD
AMSRD AMR PS PT
W CHEW
C DOLBEER
J LILLY
L FELTON
J FISHER
B MARSH
R MICHAELS
D THOMPSON
REDSTONE ARSENAL AL 35898-5249

2 PM MAS
SFAE AMO MAS
M BUTLER
BLDG 354
PICATINNY ARSENAL NJ 07806-5000

2 PM CAS
SFAE AMO CAS
BLDG 354
PICATINNY ARSENAL NJ 07806-5000

8 DIR BENET WEAPONS LAB
M AUDINO
R DILLON
R FISCELLA
R HASENBEIN
E KATHE
K MINER
S SOPOK
J MCNEIL
WATERVLIET NY 12189-4000

1 COMMANDER
RADFORD ARMY AMMO PLANT
SMCAR QA HI LIB
RADFORD VA 24141-0298

NO. OF COPIES ORGANIZATION

19 CDR US ARMY ARDEC
C ADAM BLDG 382
D CARLUCCI BLDG 94
R CARR BLDG 65N
R CIRINCIONE BLDG 171 N
S EINSTEIN BLDG 382
P HUI BLDG 382
J LANNON BLDG 1
E LOGSDEN BLDG 65S
B MACHAK BLDG B1
S NICOLICH BLDG 3022
P O'REILLY BLDG 407
J O'REILLY BLDG 382
J RUTKOWSKI BLDG 171N
A SABASTO BLDG 94
J SHIN BLDG 382
R SURAPANENI BLDG 3022
E CARAVACA BLDG 382
PICATINNY ARSENAL NJ 07806-5000

2 CDR NVL RSRCH LAB
TECH LIB
J BORIS
WASHINGTON DC 20375-5000

4 OFFICE OF NVL RSRCH
J GOLDWASSER
D SIMONS
D ROBERSON
P COLOLLY
875 N RANDOLPH ST RM 653
ARLINGTON VA 22203-1927

8 COMMANDER
NSWC
R DOHERTY R2A
C GOTZMER TM3
C MICHIENZI R22
J BUDD R22
E TERSINE R22
S MITCHELL OPA
S SMITH R3A
TECHLIB
INDIAN HEAD MD 20640-5000

NO. OF COPIES	ORGANIZATION
1	COMMANDER NSWC TECHLIB DAHLGREN VA 22448-5000
3	COMMANDER NSWC A ATWOOD S BLASHILL T PARR CH1NA LAKE CA 93555-6001
1	AIR FORCE RSRCH LAB MNME EN MAT BR B WILSON 2306 PERIMETER RD EGLIN AFB FL 32542-5910
1	AIR FORCE OFC OF SCI RSRCH M BERMAN 875 N RANDOLPH ST STE 235 RM 3112 ARLINGTON VA 22203-1768
1	NASA LANGLEY RSRCH CTR D BUSHNELL MAIL STOP 110 HAMPTON VA 23681-2199
1	DIR SANDIA NATL LABS M BAER DEPT 1512 PO BOX 5800 ALBUQUERQUE NM 87185
2	DIR LAWRENCE LIVERMORE NL L FRIED M MURPHY PO BOX 808 LIVERMORE CA 94550-0622
1	CENTRAL INTLGNC AGCY J BACKOFEN RM 4PO7 NHB WASHINGTON DC 20505
1	BATTELLE EAST SCI & TECH A ELLIS 1204 TECHLGY DR ABERDEEN MD 21001-1228
1	INST FOR ADVNCD TECHNLGY 3925 W BRAKER LN STE 400 AUSTIN TX 78759-5316

NO. OF COPIES	ORGANIZATION
2	JHU CHEM PROP INFO AGCY E LIU R FRY 10630 LITTLE PATUXENT PKWY STE 202 COLUMBIA MD 21044-3200
1 (CD only)	OUSD (AT&L)/STRAT & TACT SYS MUNITIONS T MELITA 3090 DEFNS PENTAGON RM 3 B1060 WASHINGTON DC 20301-3090
1	BRIGHAM YOUNG UNIV DEPT OF CHEM ENGRNG M BECKSTEAD PROVO UT 84601
1	CALIF INST OF TECHLGY F CULICK 204 KARMAN LAB MAIL STOP 301 46 1201 E CALIFORNIA ST PASADENA CA 91109
2	UNIV OF ILLINOIS DEPT OF MECH INDUSTRY ENGRNG H KRIER R BEDDINI 144 MEB 1206 N GREEN ST URBANA IL 61801-2978
4	PENN STATE UNIV DEPT OF MECHL ENGRNG K KUO T LITZINGER G SETTLES S THYNELL UNIVERSITY PARK PA 16802-7501
1	ARROW TECHLGY ASSOC INC 1233 SHELBURNE RD D 8 SOUTH BURLINGTON VT 05403
1	ALLEGHENY BALLISTICS LAB PO BOX 210 ROCKET CENTER WV 26726
1	ATK ORDNANCE 4700 NATHAN LN PLYMOUTH MN 55442

NO. OF
COPIES ORGANIZATION

3 ATK AMMO & ENERGETICS
RADFORD ARMY AMMO PLANT
D WORRELL
W WORRELL
S RITCHIE
RT 114 PO BOX 1
RADFORD VA 24141-0299

4 ATK THIOKOL
P BRAITHWAITE
T FARABAUGH
W WALKUP
R WARDLE
PO BOX 707
BRIGHAM CITY UT 84302-0707

1 ATK ELKTON
J HARTWELL
PO BOX 241
ELKTON MD 21921-0241

1 BAE ARMAMENT SYS DIV
J DYVIK
4800 E RIVER RD
MINNEAPOLIS MN 55421-1498

2 GEN DYNAMICS ORD/TACT SYS
N HYLTON
J BUZZETT
10101 DR M L KING ST N
ST PETERSBURG FL 33716

3 GEN DYNAMICS ST MARKS
J DRUMMOND
H RAINES
D WORTHINGTON
PO BOX 222
SAINT MARKS FL 32355-0222

1 GEN DYNAMICS ARM SYS
J TALLEY
128 LAKESIDE AVE
BURLINGTON VT 05401

3 VERITAY TECHLGY INC
R SALIZONI
J BARNES
E FISHER
4845 MILLERSPORT HWY
EAST AMHERST NY 14501-0305

NO. OF
COPIES ORGANIZATION

ABERDEEN PROVING GROUND

47 DIR USARL
AMSRD ARL WM
S MCKNIGHT
P PLOSTINS
AMSRD ARL WM B
C CANDLAND
W CIEPIELA
J B MORRIS
J NEWILL
M ZOLTOSKI
AMSRD ARL WM BA
B DAVIS
D HEPNER
G KATULKA
D LYON
AMSRD ARL WM BC
G COOPER
J DESPIRITO
F FRESCONI
J GARNER
J SAHU
S SILTON
P WEINACHT
AMSRD ARL WM BD
W ANDERSON
R BEYER
A BRANT
S BUNTE
L CHANG
J COLBURN
P CONROY
B FORCH
B HOMAN
A HORST
S HOWARD
P KASTE
A KOTLAR
K MCNESBY
M MCQUAID
A MIZIOLEK
M NUSCA (5 CPS)
R PESCE-RODRIGUEZ
B RICE
R SAUSA
E SCHMIDT
J SCHMIDT
A WILLIAMS
AMSRD ARL WM T
P BAKER
AMSRD ARL WM SG
T ROSENBERGER